Square wave operation to reduce pulsating power in isolated MMC-based ultrafast chargers

Ygor Pereira Marca, Maurice G. L. Roes, Jorge L. Duarte and Korneel Wijnands
Eindhoven University of Technology
Electromechanics and Power Electronics Group
P.O. Box 513, 5600MB
Eindhoven, The Netherlands
Phone: +31 (0) 61-377-4267
Email: y.pereira.marca@tue.nl

Acknowledgments

This publication is part of the project NEON (with project number 17628 of the research programme Crossover which is (partly) financed by the Dutch Research Council (NWO)).

Keywords

≪Charger≫, ≪Full-bridge sub-modules≫, ≪Medium-frequency transformer≫, ≪Medium-voltage grid≫, ≪Modular multilevel converter≫, ≪Square wave≫.

Abstract

This paper presents an application of modular multilevel converters to reduce pulsating power, and therefore sub-modules in ultrafast chargers. The converter's analysis and a control scheme were presented to realize bidirectional power transfer between a three-phase medium-voltage grid and a single-phase medium-frequency transformer with square-shaped voltage, successfully reducing power fluctuation.

Introduction

Due to its modularity, output voltage quality, and high efficiency, the modular multilevel converter (MMC) has been widely used for medium-voltage and high-power conversion since its first publication in [1]. Its configuration is scalable to satisfy different voltage and power demands. Furthermore, the voltage over semiconductors is minimized because sub-modules are connected in series [2].

Recently, ultrafast chargers implementing ac/ac MMC are being researched to reduce cost and size in medium-voltage applications. As shown in Fig. 1, a medium-frequency transformer can be integrated into the MMC-based charger to substitute the bulky line-frequency transformer that is normally used for electrical isolation [3]. Furthermore, by use of a proper transformer current control, switching losses in the ac/dc converter (Fig. 1) can be reduced [4, 5]. Yet, the single-phase output of the MMC inherently leads to power fluctuation, which increases the medium-frequency transformer losses and size of capacitor [6, 7]. Therefore, it is appropriate to evaluate and propose a strategy to decrease pulsating power in such a system.

Previous research has shown the possibility of creating a square instead of a sinusoidal voltage waveform on the MMC single-phase terminals [8,9]. Square-shaped current and voltage quantities reduce pulsating power in medium-voltage chargers [10]. Therefore, this paper presents a strategy to implement the square-shaped voltage waveform in the MMC single-phase terminals. The proposed system increases the efficiency and power density of ultrafast charging stations.

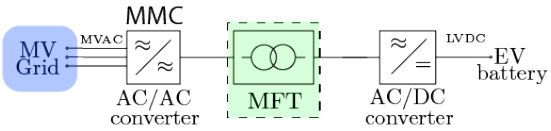

Fig. 1: MMC-based ultrafast charger with a medium-frequency transformer.

Modular multilevel converter

For each of the three phases indexed by $y \in \{a, b, c\}$, there is an upper and a lower arm indicated by $\mathrm{x} \in \{\mathrm{u}, \ell\}$. The arms are composed of N series-connected sub-modules, all of which contain a full-bridge converter and a capacitor as shown in Fig. 2. The MMC based on full-bridge sub-modules can generate any periodic voltage waveform over the single-phase medium-frequency transformer terminals [11]. However, the amplitude is limited by the converter's voltage rating, which can be chosen to obtain high efficiency [3].

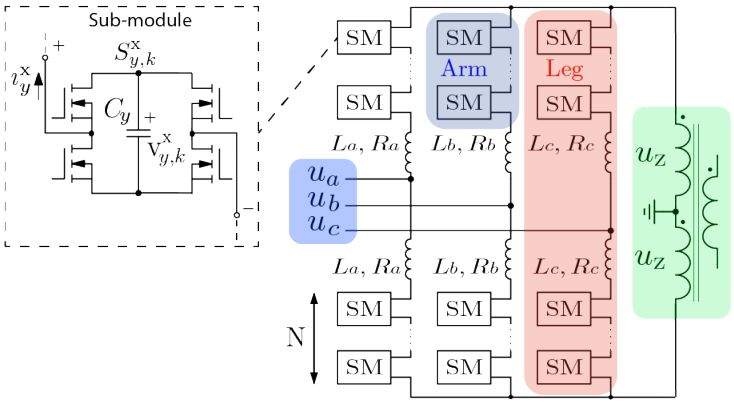

Fig. 2: Three-phase to single-phase ac/ac MMC with full-bridge sub-modules.

Fundamentals

Controllable average voltage sources can be used to represent the average behavior of all sub-modules in an arm to simplify the analysis, as shown in Fig. 3. In addition, each arm has a series inductance to allow current control [2].

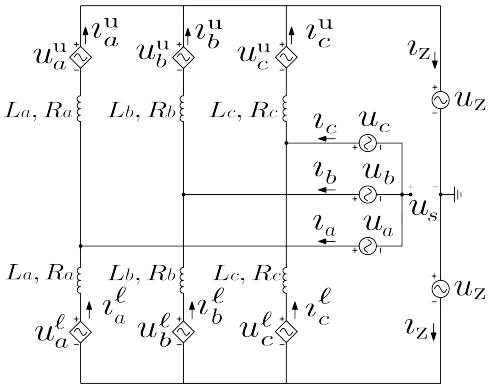

Fig. 3: Three-phase to single-phase ac/ac MMC equivalent circuit.

As described in [3], it is favorable to separate the arm currents into components, namely, common-mode current ($\imath_y^{\Sigma}$) and differential-mode current ($\imath_y^{\Delta}$), as

$$\imath_y^{\Sigma} = \frac{1}{2}\left(\imath_y^{\mathrm{u}} + \imath_y^{\ell}\right), \tag{1}$$

$$\imath_y^{\Delta} = \frac{1}{2}\left(\imath_y^{\mathrm{u}} - \imath_y^{\ell}\right). \tag{2}$$

In the same manner, the arm voltages are split into common-mode (u_y^{Σ}) and differential-mode voltage (u_y^{Δ}), as

$$u_y^{\Sigma} = \frac{1}{2}\left(u_y^{\mathrm{u}} + u_y^{\ell}\right), \tag{3}$$

$$u_y^{\Delta} = \frac{1}{2}\left(u_y^{\mathrm{u}} - u_y^{\ell}\right). \tag{4}$$

Using these definitions, the circuit differential equations can be written with common-mode and differential-mode components. Then, Kirchhoff's voltage law applied to the upper and lower loops results in

$$L_y \frac{d}{dt} i_y^{\Sigma} + R_y i_y^{\Sigma} = u_y^{\Sigma} - u_{\mathrm{z}}, \tag{5}$$

$$L_y \frac{d}{dt} i_y^{\Delta} + R_y i_y^{\Delta} = u_y^{\Delta} + u_y. \tag{6}$$

The arm voltages u_y^{x} can be used to control the common-mode and differential-mode currents. These voltages are the result of the output voltages of N series-connected sub-modules as $u_y^x = \sum_{k=1}^{N} S_{y,k}^x \mathrm{v}_{y,k}^{\mathrm{x}}$, with the k^{th} sub-module's switching function given by $S_{y,k}^{\mathrm{x}} \in \{-1, 0, 1\}$ and $\mathrm{v}_y^{\mathrm{x}}$ the k^{th} sub-module's capacitor voltage. In addition, a control scheme is required to balance sub-modules' capacitor voltage [2].

Power distribution

For stable operation, each converter leg must deliver or receive a constant average power to the three-phase or single-phase terminals, regardless of their voltage and current waveforms. Furthermore, the average power difference between the upper and lower arms must be zero to keep the converter balanced.

Based on the instantaneous power $p_y^{\mathrm{x}} = -u_y^{\mathrm{x}} i_y^{\mathrm{x}}$ processed by each controllable voltage source in Fig. 3, it is convenient to define in line with (1)-(2),

$$p_y^{\Sigma} = \frac{1}{2}\left(p_y^{\mathrm{u}} + p_y^{\ell}\right), \tag{7}$$

$$p_y^{\Delta} = \frac{1}{2}\left(p_y^{\mathrm{u}} - p_y^{\ell}\right). \tag{8}$$

The differential-mode components are related to the grid with frequency ω_1 [3]. Assuming that the grid voltages and currents are sinusoidal, we have that

$$-u_y^{\Delta} = \sqrt{2} U_y^{\Delta} \cos\left(\omega_1 t + \theta_y^{\Delta}\right), \tag{9}$$

$$i_y^{\Delta} = \sqrt{2} I_y^{\Delta} \cos\left(\omega_1 t + \varphi_y^{\Delta}\right). \tag{10}$$

Then, after some manipulations (7) and (8) result in

$$p_y^{\Sigma} = 2 U_y^{\Delta} \cos\left(\omega_1 t + \theta_y^{\Delta}\right) I_y^{\Delta} \cos\left(\omega_1 t + \varphi_y^{\Delta}\right) - u_y^{\Sigma} i_y^{\Sigma}, \tag{11}$$

$$p_y^{\Delta} = \sqrt{2} U_y^{\Delta} \cos\left(\omega_1 t + \theta_y^{\Delta}\right) i_y^{\Sigma} - \sqrt{2} I_y^{\Delta} \cos\left(\omega_1 t + \varphi_y^{\Delta}\right) u_y^{\Sigma}. \tag{12}$$

This common-mode and differential-mode power must be controlled, to have in steady-state operation the averages $P_y^{\Sigma} = P_y^{\Delta} = 0$.

Efficiency

According to [3], an estimation of the charger efficiency can be determined by considering the switch conduction losses. The required number of sub-modules per arm and the derated maximal voltage of the switches are given by

$$N = \left\lceil \frac{\widehat{U}_y + \widehat{U}_{\mathrm{z}}}{\mathrm{V}_{sw}} \right\rceil, \tag{13}$$

$$\mathrm{V}_{sw} = \mathrm{V}_{ds} D_F, \tag{14}$$

where V_{ds} and D_F are the semiconductor device breakdown voltage and derating factor, respectively. Switching losses may be disregarded in efficiency evaluation when considering SiC MOSFETs that are operated at sufficiently low switching frequencies. Therefore, given the RMS arm currents [3], $I_y^{\mathrm{x}} = \sqrt{\frac{I_y^2}{4} + \frac{I_z^2}{9}}$, the total conduction losses and power efficiency of the ac/ac MMC are approximated by

$$P_{\mathrm{loss}} = 12 R_{ds} N (I_y^{\mathrm{x}})^2, \tag{15}$$

$$\eta = \left(1 - \frac{P_{\mathrm{loss}}}{P}\right) \cdot 100, \tag{16}$$

where R_{ds} is the on-state resistance of each switch in a sub-module and P is the charger's nominal processed power.

MMC control

The proposed scheme controls the bidirectional power flow between the three-phase and single-phase terminals of the ac/ac MMC as well as the sub-modules capacitor voltages. The power exchange with the grid can be regulated through a PQ controller of frequency ω_1 [12], and the power exchange with the transformer terminals can be controlled through a PQ controller of frequency ω_2 or as presented in [3].

Internal and square wave current control

Maintaining all capacitor voltages ($\mathrm{v}_{y,k}^{\mathrm{x}}$) balanced around a reference is a requirement for the MMC's stable operation [12, 13]. As analyzed in (11) and (12), two independent components must be introduced in u_y^{Σ}, and therefore also in $\imath_y^{\Sigma}$, with frequencies ω_1 and ω_2 for decoupled control. Frequency ω_1 is related to the three-phase grid, and frequency ω_2 corresponds to the (fundamental) frequency of the single-phase medium-frequency transformer terminal voltage. So, common-mode components are introduced as

$$u_y^{\Sigma} = \sqrt{2} U_{y1}^{\Sigma} \cos\left(\omega_1 t + \theta_{y1}^{\Sigma}\right) + \sqrt{2} U_{y2}^{\Sigma} \cos\left(\omega_2 t + \theta_{y2}^{\Sigma}\right), \tag{17}$$

leading to

$$\imath_y^{\Sigma} = \sqrt{2} I_{y1}^{\Sigma} \cos\left(\omega_1 t + \varphi_{y1}^{\Sigma}\right) + \sqrt{2} I_{y2}^{\Sigma} \cos\left(\omega_2 t + \varphi_{y2}^{\Sigma}\right). \tag{18}$$

While components with frequency ω_1 are necessary to regulate the imbalance in the capacitor voltages that occurs due to the three-phase grid currents, components with frequency ω_2 are needed to control power transfer with single-phase terminals and the imbalance that this creates in the MMC. Therefore, given that $\varphi_{y1}^{\Sigma} = \theta_{y1}^{\Sigma} - \frac{\pi}{2}$ due to the MMC arm inductance, and imposing $\theta_{y1}^{\Sigma} = \theta_y^{\Delta}$, the substitution of (17) and (18) into (11) and (12) results in the average common-mode and differential-mode power

$$P_y^{\Sigma} = U_y^{\Delta} I_y^{\Delta} \cos\left(\theta_y^{\Delta} - \varphi_y^{\Delta}\right) - U_{y2}^{\Sigma} I_{y2}^{\Sigma} \cos\left(\theta_{y2}^{\Sigma} - \varphi_{y2}^{\Sigma}\right), \tag{19}$$

$$P_y^{\Delta} = -U_{y1}^{\Sigma} I_y^{\Delta} \cos\left(\theta_y^{\Delta} - \varphi_y^{\Delta}\right). \tag{20}$$

The average power P_y^{Σ} in (19) is equal to the difference between the three-phase and single-phase terminal powers. This difference should be made equal to zero during steady-state by controlling the power transfer. In addition, P_y^{Δ} in (20) will be regulated by U_{y1}^{Σ}. In steady-state $U_{y1}^{\Sigma} = 0$ and $I_{y1}^{\Sigma} = 0$. Therefore, in view of (19) and (20), u_y^{Σ} and u_y^{Δ} can be controlled through P_y^{Σ} and P_y^{Δ}. Numerous control schemes are capable of balancing the MMC arms' average power, as presented for example in [3, 4, 12, 13]. However, it is not covered in this paper. The diagram presented in Fig. 4 is responsible for shaping the voltage and current quantities of the single-phase transformer terminals into square waveforms to mitigate pulsating power in ultrafast chargers. The influence of shaping sinusoidal into square waves on the capacitor voltage control is negligible because the average remains $P_y^{\Sigma} = P_y^{\Delta} = 0$ after modifying (17) in Fig. 4.

The references $u_{y1}^{\Sigma *}$ and $u_{y2}^{\Sigma *}$ in Fig. 4 are given by an internal balance control needed to regulate capacitors' voltage [3, 12]. Then, to obtain a medium-frequency transformer with square-shaped quantities,

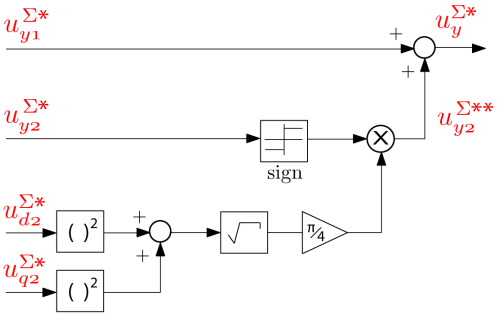

Fig. 4: Control scheme for a square-shaped medium-frequency transformer voltage.

$u_{y2}^{\Sigma*}$ is modified as presented in Fig. 4. The sign function transforms the sinusoidal waveform with angle θ_{y2}^{Σ} into a square wave. The dq voltages $u_{d2}^{\Sigma*}$ and $u_{q2}^{\Sigma*}$ from the PQ control of the single-phase terminals give the square wave amplitude. As a result, both $u_{y1}^{\Sigma*}$ and $u_{y2}^{\Sigma**}$ create the common-mode voltages and currents that modify (17) and (18), and therefore (19) and (20), successfully resulting in a square-shaped voltage and current on the single-phase side.

Simulation results

Simulations were conducted with the averaged equivalent circuit shown in Fig. 3. The capacitors in each arm are assumed to be equal, therefore the total equivalent arm capacitance C_σ is equal to $C_\sigma = \frac{C_y}{N}$, where C_y is the capacitance of each sub-module. The capacitors' voltage is stabilized around a reference by means of control. The main system parameters are described in Table I.

Table I: Ratings of the simulated three-phase to single-phase ac/ac MMC.

Description	Variable	Value	Unit
Charger nominal power	P	1	MW
Phase-to-neutral RMS voltage	U_y	$25\sqrt{1/3}$	kV
Grid frequency	f_1	50	Hz
Transformer RMS voltage	U_z	5	kV
Transformer frequency	f_2	1	kHz
Arm capacitance	C_σ	250	uF
Arm inductance	L_y	1	mH
Arm resistance	R_y	0.05	Ω
MOSFET on-resistance	R_{ds}	20	mΩ
MOSFET breakdown voltage	V_{ds}	1.2	kV
MOSFET derating factor	D_F	75	%

According to (3) and (4), the arm voltages contain components with frequencies ω_1 and ω_2 from the grid and medium-frequency transformer terminals, respectively. Fig. 5 illustrates the arm voltages produced by the common-mode and differential-mode voltages. Moreover, the square-shaped transformer current control can be made by generating common-mode voltage references $u_y^{\Sigma*}$ as presented in Fig. 4 and attested in Fig. 6. However, square wave voltage reduces the possible number of voltage levels in the MMC, leading to higher dv/dt on sub-modules and medium-frequency transformer.

Fig. 7 illustrates the stabilized capacitor voltages that act as energy buffers between both ac terminals and Fig. 8 shows purely sinusoidal three-phase grid currents, validating the steady-state operation of the ac/ac MMC. Since both frequencies are decoupled in the common-mode and differential-mode components, the medium frequency ω_2 is not reflected to the grid terminals, and therefore, filters are not required [14].

The amplitude and RMS values of a square-shaped voltage are equal, while the amplitude of a sinusoidal

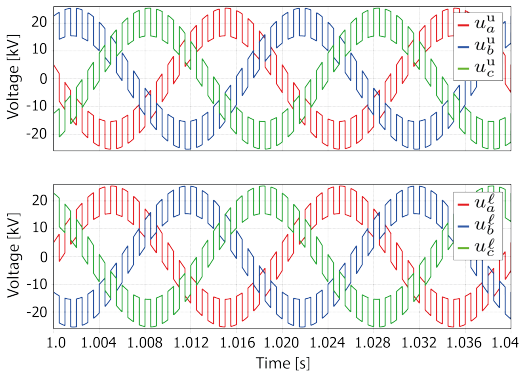

Fig. 5: MMC arm voltages.

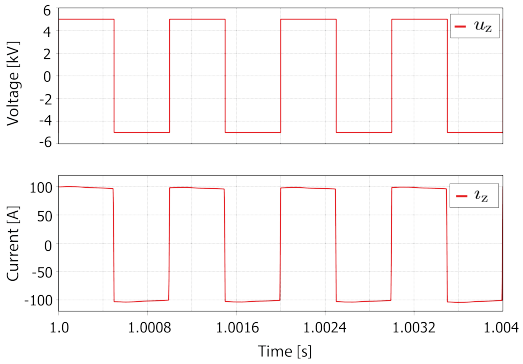

Fig. 6: Transformer square-shaped quantities.

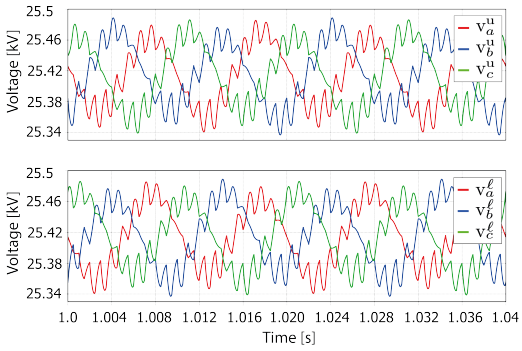

Fig. 7: Summed capacitor voltage of MMC arms.

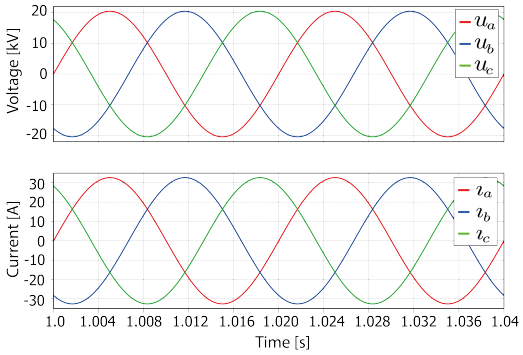

Fig. 8: Three-phase grid voltages and currents.

wave is higher than its RMS value. Therefore, the instantaneous power of square-shaped quantities is equal to the average, while sinusoidal-shaped power has a higher pulsation [10]. In addition, square-shaped voltage increases the utilization of components in MMC, because as presented in (13), square wave quantities require fewer sub-modules than sinusoidal waves, meaning higher efficiency and power density. For instance, (13) and (16) are presented in Fig. 9 for both square-shaped and sinusoidal single-phase voltages with ratings shown in Table I. Note that above $U_{\mathrm{z}} = 5\mathrm{kV}$, conduction losses represent less than 1% of the processed power and sub-modules are reduced with square-shaped voltage.

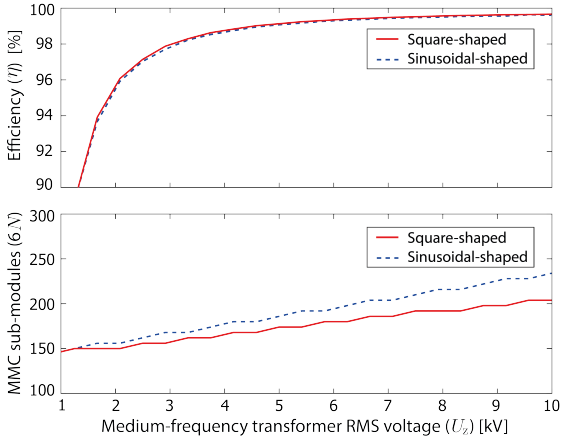

Fig. 9: MMC efficiency and number of sub-modules in relation to the transformer RMS voltage.

Conclusion

In order to decrease pulsating power in ultrafast charging stations, an ac/ac MMC connected to a medium-frequency transformer with a square wave voltage output was proposed in this paper. Using the presented strategy, a three-phase grid voltage can be converted into a medium-frequency square-shaped voltage. As a result, the application decreases cost and volume of high-power chargers by replacing line-frequency with medium-frequency transformers. However, the application has the disadvantage of increasing dv/dt on the MMC sub-modules and transformer terminals.

Simulations show the power exchange with the single-phase medium-frequency transformer using square wave voltage output, while keeping the capacitor voltages regulated. Transferring power with square-shaped voltage and current reduces pulsating power in single-phase systems. In this paper, the pulsating power reduction is quantified by the decrease in sub-modules of MMC-based chargers. Furthermore, as the model decouples frequencies from the grid and transformer terminals, filters are not necessary to comply with harmonic emission requirements.

References

[1] R. Marquardt, A. Lesnicar, J. Hildinger *et al.*, "Modulares stromrichterkonzept für netzkupplungsanwendung bei hohen spannungen," *ETG-Fachtagung, Bad Nauheim, Germany*, vol. 114, 2002.

[2] A. Antonopoulos, L. Angquist, and H.-P. Nee, "On dynamics and voltage control of the modular multilevel converter," in *2009 13th European Conference on Power Electronics and Applications*. IEEE, 2009, pp. 1–10.

[3] Y. P. Marca, M. G. L. Roes, J. L. Duarte, and C. G. E. Wijnands, "Isolated MMC-based ac/ac stage for ultrafast chargers," in *IEEE-ISIE2021-30th International Symposium on Industrial Electronics-Kyoto*. Institute of Electrical and Electronics Engineers, 2021.

[4] M. Schnarrenberger, F. Kammerer, M. Gommeringer, J. Kolb, and M. Braun, "Current control and energy balancing of a square-wave powered 1AC-3AC modular multilevel converter," in *2015 IEEE Energy Conversion Congress and Exposition (ECCE)*. IEEE, 2015, pp. 3607–3614.

[5] M. Schnarrenberger, F. Kammerer, D. Bräckle, and M. Braun, "Cell design of a square-wave powered 1AC-3AC modular multilevel converter low voltage prototype," in *2016 18th European Conference on Power Electronics and Applications (EPE'16 ECCE Europe)*. IEEE, 2016, pp. 1–11.

[6] R. Agarwal, S. Martin, Y. Shi, and H. Li, "High frequency transformer core loss analysis in isolated modular multilevel DC-DC converter for MVDC application," in *2019 IEEE Energy Conversion Congress and Exposition (ECCE)*. IEEE, 2019, pp. 6419–6423.

[7] R. Mo, H. Li, and Y. Shi, "A phase-shifted square wave modulation (PS-SWM) for modular multilevel converter (MMC) and dc transformer for medium voltage applications," *IEEE Transactions on Power Electronics*, vol. 34, no. 7, pp. 6004–6008, 2018.

[8] M. Glinka and R. Marquardt, "A new AC/AC-multilevel converter family applied to a single-phase converter," in *The Fifth International Conference on Power Electronics and Drive Systems, 2003. PEDS 2003.*, vol. 1. IEEE, 2003, pp. 16–23.

[9] M. Glinka, "Prototype of multiphase modular-multilevel-converter with 2 MW power rating and 17-level-output-voltage," in *2004 IEEE 35th Annual Power Electronics Specialists Conference (IEEE Cat. No. 04CH37551)*, vol. 4. IEEE, 2004, pp. 2572–2576.

[10] K. Pouresmaeil, J. L. Duarte, C. G. E. Wijnands, M. G. L. Roes, and N. H. Baars, "Single-phase bidirectional ZVZCS AC-DC converter for MV-connected ultra-fast chargers," in *PCIM Europe 2022*. VDE Verlag, 2022, pp. 124–130.

[11] G. Mondal and S. Nielebock, "Control of M2C direct converter for AC to AC conversion with wide frequency range," in *2016 18th European Conference on Power Electronics and Applications (EPE'16 ECCE Europe)*. IEEE, 2016, pp. 1–10.

[12] L. Bessegato, K. Ilves, L. Harnefors, S. Norrga, and S. Östlund, "Control and admittance modeling of an ac/ac modular multilevel converter for railway supplies," *IEEE transactions on power electronics*, vol. 35, no. 3, pp. 2411–2423, 2019.

[13] K. Sharifabadi, L. Harnefors, H.-P. Nee, S. Norrga, and R. Teodorescu, *Design, control, and application of modular multilevel converters for HVDC transmission systems*. John Wiley & Sons, 2016.

[14] F. Rojas, M. Diaz, M. Espinoza, and R. Cárdenas, "A solid state transformer based on a three-phase to single-phase modular multilevel converter for power distribution networks," in *2017 IEEE Southern Power Electronics Conference (SPEC)*. IEEE, 2017, pp. 1–6.